

Nanomechanical sensors for single microbial cell growth monitoring†

Cite this: *Nanoscale*, 2014, 6, 8242

Niall Maloney,‡ Gyongyi Lukacs,‡ Jason Jensen and Martin Hegner*

A nanomechanical technique for rapid real time detection and monitoring of microorganism growth will significantly reduce costs and diagnosis times in industrial and clinical settings. Owing to their label free detection mechanism and unprecedented sensitivity to the mass and elastic modulus of biological structures, dynamically operated cantilever arrays provide an opportunity to rapidly detect and track the evolution of microbial growth. Here we report the monitoring of the growth of single *Aspergillus niger* spores *via* the multimode response of microcantilevers. The fungal hyphal structure affects the cantilevers' nanomechanical properties as it propagates along the sensor. We demonstrate, for the first time, the mapping of cellular events with great accuracy using a cantilever frequency response. Imaging of growth conditions on the cantilever, which is performed in parallel, allows for verification of these results. Theoretical comparison and finite element modelling confirm experimental findings and allow for determination of the hyphal elastic modulus.

Received 24th March 2014
Accepted 9th May 2014

DOI: 10.1039/c4nr01610f

www.rsc.org/nanoscale

Introduction

Monitoring of microorganism growth is a requirement in regulated and controlled manufacturing environments in areas such as the health, pharmaceutical, and food industries. In the past three decades the incidence of fungal infection has increased dramatically. Pharmaceutical and food industries require the culturing of bacteria and microfungi as part of quality controls for preservative testing,¹ while monitoring of both the fermenting microbe² and any possible contaminants³ is essential for fermentation technologies. Traditional detection methods such as plate counting, polymerase chain reaction (PCR), microtiter broth dilutions, and microscopy are time consuming, labour intensive, and suffer from live/dead cell discrimination issues (PCR). Thus, there is a need for the development of technologies which are capable of the real time monitoring of fungal growth in a rapid and reliable fashion. Advancements in nanotechnology have allowed for the development of biosensors for pathogen detection with detection mechanisms *via* optical,⁴ electrical,⁵ or mechanical⁶ means.

The advent of the atomic force microscope (AFM) in the 1980s⁷ created the availability of micron sized cantilevers. A vast improvement in silicon processing technologies in the intervening decades has resulted in the reproducible production of relatively inexpensive high quality cantilevers. While

traditionally used as surface probes, pioneering work performed simultaneously by research groups in Europe,⁸ and the USA⁹ in the 1990s saw the first use of cantilevers for physical and chemical sensing applications. Since then published reports detailing the use of cantilevers for sensing have increased greatly. Typically the static deflection (static mode) or resonance frequency (dynamic mode) of a cantilever is tracked with respect to time.¹⁰ Recently devices capable of both modes of operation have been developed.¹¹ When operated in dynamic mode a cantilever is traditionally thought of as a mass sensor where mass loading on the cantilever produces a negative resonance frequency shift. The mass sensitivity of a cantilever sensor is seen to be enhanced when higher order modes of vibration are utilised.¹² Further development of sensor fabrication techniques has resulted in nanoscale cantilevers which have achieved a mass resolution of 1 ag ($a = 10^{-18}$) under ambient conditions.¹³

The unprecedented sensitivity offered by cantilevers has resulted in their emergence as biological sensors in the last 15 years. The biggest advantage of using these sensors is that they allow for label free detection to be performed. The use of cantilevers in static mode has been reported in the fields of proteomics^{14,15} and genomics.^{16,17} The detection of single virus particles¹⁸ and the binding of bacteriophage particles¹⁹ have been demonstrated using cantilever resonators.

Cantilever resonators have previously been employed for the detection of microbial pathogens. In the majority of cases cells are captured from suspensions using different immobilisation techniques. Typically antibody-antigen immobilisation is employed,^{20,21} however the use of poly-L-lysine²² and α -D-mannose²³ functionalised sensors has been reported. The

Centre for Research on Adaptive Nanostructures and Nanodevices (CRANN), School of Physics, Trinity College Dublin, Dublin 2, Ireland. E-mail: martin.hegner@tcd.ie

† Electronic supplementary information (ESI) available. See DOI: 10.1039/c4nr01610f

‡ Contributed equally to this work.

main drawback of using cantilevers for pathogen detection is not in regards to sensitivity or specificity, which outperforms other currently used techniques, but their inability to distinguish between live and dead cells.

In order to overcome the difficulty of live/dead cell discrimination cantilevers have been employed for the real time monitoring of microbe growth. A limited number of studies have been published outlining the use of cantilever sensors in this fashion with all but two^{24,25} employing the dynamic mode of operation for detection. By this method cells are deposited onto the cantilever sensor, which is then exposed to conditions which are suitable for growth. The group of Mutharasan performed single sensor measurements using relatively large piezoelectric-excited millimetre-sized cantilevers (PEMCS) for the detection of *Escherichia coli* (*E. coli*) in both air²⁶ and liquid.²⁷ These measurements^{24–27} were performed without the use of *in situ* reference sensors which allow for the elimination of false positive environmental signals that all cantilever measurements are susceptible to. Cell multiplication results in resonance frequency shifts, which allow for the detection of growth faster than conventional growth detection methods. The use of hydrogel functionalised cantilever arrays for the detection of the growth of *E. coli*²⁸ and *Aspergillus niger* (*A. niger*)^{29,30} has also been reported. By this method nutritional medium is held in an agarose matrix onto which cells are deposited.³¹ The array is then placed into a humid environment where absorption/adsorption of water by/on the newly formed biomaterial results in a resonance frequency shift. *In situ* reference sensors enable unambiguous differential analysis where the response of the reference sensor can be deduced from the response of the sensor to deconvolute signals which are not arising from viable growth.

Traditionally, the adsorption of a particle with mass (m_a) was thought to produce a negative resonance frequency shift (Δf_n) as shown in eqn (1)

$$\frac{\Delta f_n}{f_{0n}} = \frac{\psi_n^2(x)}{2} \frac{m_a}{m_b} \quad (1)$$

where $\psi_n(x)$ is the amplitude of the n^{th} mode of vibration at a position (x) along the cantilevers' longitudinal axis.³² The subscripts a and b indicate the adsorbate and cantilever beam respectively. From eqn (1) it is clear that the magnitude of Δf_n is proportional to the square of the amplitude of vibration at that position (x). It has been shown that the adsorption of particles on a cantilever can produce a positive shift in resonance frequency. It is proposed that the stiffness (Young's modulus) of the adsorbed material alters the flexural rigidity of the cantilever. Thus, eqn (1) must be modified to account for this change in flexural rigidity as follows,

$$\frac{\Delta f_n}{f_{0n}} = \left(\frac{3}{2} \frac{1}{\beta_n^4} \frac{d^2 \psi_n(\delta)^2}{d\delta^2} \frac{E_a}{E_b} - \frac{1}{2} \psi_n^2(\delta) \frac{\rho_a}{\rho_b} \right) \frac{V_a}{V_b} \quad (2)$$

where E , ρ , V and β_n correspond to Young's modulus, density, volume, and eigenvalues respectively.^{32–34} δ is the x -coordinate normalized by the beam length (L). Eqn (2) reveals that responsivity due to the stiffness of the adsorbate is proportional to the curvature of the vibration mode shape, $d^2 \psi_n(\delta)^2 / d\delta^2$, at the adsorption position. Fig. 1 shows plots of mode shape (black

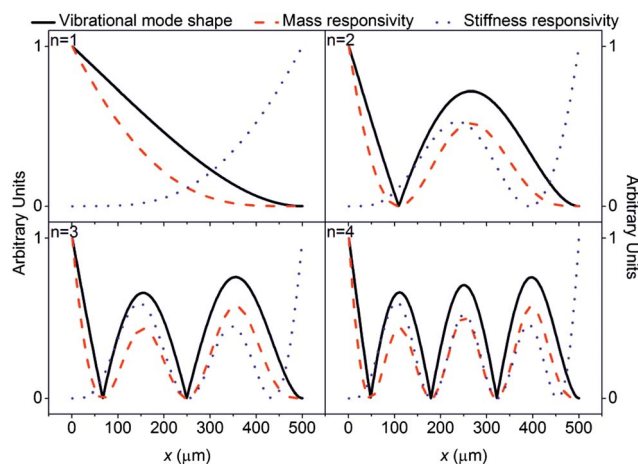


Fig. 1 Mode shape (solid black line) and responsivity due to the mass (dashed red line) and stiffness effect (blue dotted line) for the first four flexural resonance modes. x corresponds to the length along the cantilevers' longitudinal axis. $x = 0$ corresponds to the cantilevers' free end and $x = 500$ to the clamped end. These curves are plots of $\psi_n(x)$ (solid black line), $\psi_n^2(x)$ (dashed red line), and $d^2 \psi_n(x)^2 / d(x)^2$ (blue dotted line) which represent vibrational amplitude, proportionality to mass sensitivity (amplitude squared), and proportionality to stiffness sensitivity (curvature squared) respectively.

line) with mass (red dash) and stiffness responsivities (blue dot) for the first four flexural resonance modes. The mass and stiffness effects are decoupled at the free and clamped ends of the cantilever respectively. In between these points resonance frequency shifts have both mass and stiffness components. Detailed discussion of these effects can be found in ref. 32 and 34. Deposited bacterial cells have been shown to cause positive shifts in resonance frequency.^{33,34} The growth of *A. niger* proceeds *via* the spreading of hyphal filaments. These are tubular structures, with a diameter of approximately $5 \mu\text{m}$, that play a crucial role in the colonisation of a substrate. Hyphal growth on cantilevers has been shown to produce positive and negative resonance frequency shifts.³⁵

Here the utilisation of hydrogel functionalised cantilevers for the monitoring of single *A. niger* spore growth is presented using an identical device to that reported in ref. 35. Parallel imaging of conditions on the cantilever surface is performed to provide a link between the multimode frequency response of cantilever sensors and the progression of hyphal growth along the sensor length.

Results and discussion

Fungal growth on $7 \mu\text{m}$ thick cantilevers

Fig. 2(a) shows the relative fundamental and second mode resonance frequency shifts for three test cantilevers, onto which individual spores have been placed, and two agarose coated reference cantilevers. Test cantilevers show a clear divergence from the constant frequency drift observed for reference sensors. Therefore, it is possible to conclude that growth of single *A. niger* spores has been detected within 7–10 hours. This time is an order of magnitude faster than conventional growth

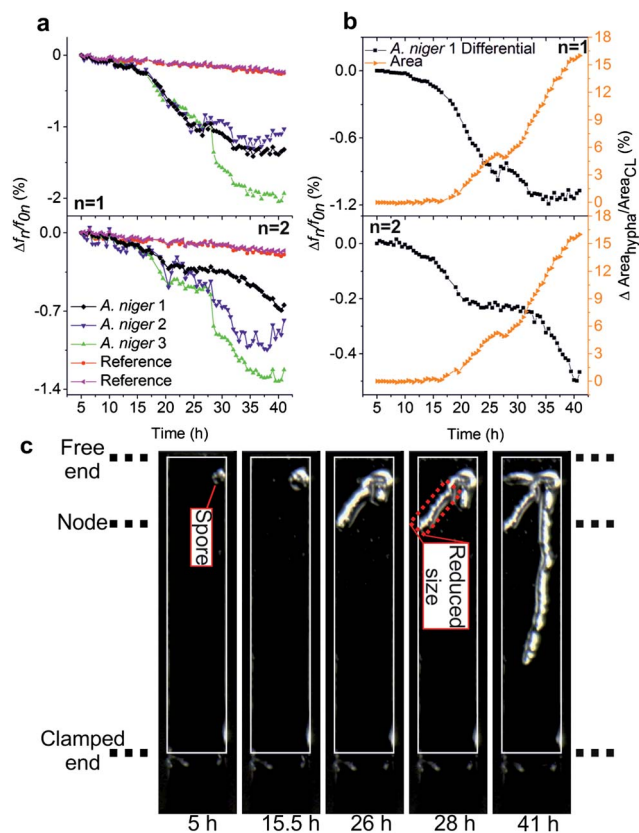


Fig. 2 Data concerning growth measurement performed using 7 μm thick cantilevers. (a) Relative resonance frequency shift of reference and test cantilevers (*A. niger* 1, 2, 3). There is a change in resonance frequency of test cantilevers compared to reference sensors. Plots are shown for the fundamental and the second resonance mode. (b) Differential fundamental and second mode relative frequency shifts of *A. niger* 1. The orange data points represent the percentage change in hyphal coverage of the cantilever. (c) Images of growth conditions on the cantilever during the measurement. White rectangles outline the cantilever. The free and the clamped end of the cantilever beam are indicated to both sides of images. The node of vibration for the second resonance mode is also indicated.

detection techniques which rely on the visual observation of the fungal mycelium.

Fig. 2(b) shows the differential resonance frequency shift for the fundamental and second resonance modes of cantilever *A. niger* 1. Sensors *A. niger* 2 and *A. niger* 3 are not discussed, however, similar observations can be made to explain resonance frequency shifts. The orange data points on these plots correspond to the change in hyphal coverage of the cantilever ($\Delta \text{Area}_{\text{hypha}}/\text{Area}_{\text{CL}}$). The hyphal area was obtained from recorded images using National Instruments IMAQ vision acquisition software. In the case of the fundamental resonance mode there is a correlation between increases in hyphal coverage and negative resonance frequency shifts.

Different rates of resonance frequency change can be explained through examination of the images shown in Fig. 2(c). Between 5 and 15.5 hours there is significant spore swelling which is reflected in a resonance frequency decrease. The increase in spore size, due to the intake of water by the

cytoplasm, results in increased water adsorption on the hydrophilic outer wall of the spore. Swelling occurs prior to generation of the germ tube which leads the way for hypha formation.^{36,37} After spore swelling hyphal filaments begin to spread towards the cantilevers' clamped end, resulting in an increased rate of resonance frequency change. The resonance frequency continues to decrease at a linear rate until 26.5 hours, where an increase in resonance frequency is observed. Examination of the hyphal coverage plot (Fig. 2(b)) reveals a decrease in coverage at this time point. This is indicative of the mass loss on the cantilever. Through inspection of images marked 26 and 28 hours it can be seen that the hypha marked in red has significantly reduced in size. This reduction in size appears to be due to a loss of liquid, which is adsorbed on the hypha outer wall. Partial drying appears to affect this specific hypha while the rest of the fungal structure retains its full water layer. It is postulated that this drying is due to the secretion of proteins known as hydrophobins. Hydrophobins form amphipathic monolayers at hydrophobic-hydrophilic interfaces which reduce the surface tension of the medium or the substrate in/on which fungi grow.³⁸ This reduction in surface tension ensures that hyphae can form structures such as aerial hyphae or fruiting bodies. The hydrophilic side of the hydrophobin faces the hypha cell wall whereas the hydrophobic rodlet-decorated surface is exposed to air.³⁹ The hypha discussed here fails to emerge into air but is no longer able to assimilate nutrition from the humid environment and thus ceases to grow further.

Two additional hyphal filaments emerge from the spore, one which propagates towards the cantilevers' clamped end and one towards the left of the cantilever. In the case of the fundamental resonance mode at 34.5 hours no further negative frequency shift is observed, however, fungal growth still occurs. This indicates that the hyphal tip has propagated into a region of the cantilever length where the amplitude of vibration is insufficient to produce a negative resonance frequency shift. No positive frequency shift is observed. This indicates that the stiffness contribution of the hypha in question on sensor *A. niger* 1 is negligible compared to the high Young's modulus 7 μm thick measurement sensor.

In the case of the second resonance mode hyphal swelling and spore germination are seen to produce negative frequency shifts, as was the case for the fundamental mode. Between the time points of 22 and 32.5 hours there seems to be a constant resonance frequency. From examination of the recorded images and the plot of hyphal coverage of the cantilever, it is clear that fungal growth occurs during these time points. Thus, it is possible to conclude that growth occurs in a region of the cantilever length which does not have sufficient amplitude to produce a measurable resonance frequency shift (see also Fig. 1 ($n = 2$), vibrational node at position $\sim 112 \mu\text{m}$ from the cantilevers' free end). This occurs at the node of vibration on the sensor, which is indicated beside the images in Fig. 2(c). The rise in resonance frequency observed in the fundamental resonance mode at 26.5 hours is not detectable in the case of the second resonance mode. This is due to the fact that the hypha, which suffers from a reduction in its surrounding water layer, is located in this mass insensitive region. A negative resonance

frequency shift is observed after 32.5 hours, indicating that hyphal growth has entered a mass sensitive region once again. A time lapse video of the evolution of fungal growth on the cantilever sensors can be found in the ESI (see Movie S1†).

Tracking more than one resonance mode provides information regarding the position, (x), of the hyphal tip along the cantilevers' longitudinal axis, whilst also providing a qualitative growth detection result. We observed that growth through regions of low vibrational amplitude results in decreased mass sensitivity. Evaluation of resonance frequency allows for the position of the hyphal tip to be determined. For example, in the case of the fundamental mode a reduction in mass sensitivity is observed as the hyphal tip approaches the mid-point of the cantilevers' longitudinal axis. At the same time, in the case of the second resonance mode mass sensitivity decreases in the vicinity of the vibrational nodes.^{32–34} Hence, measurement of both resonance modes reveals that hyphal propagation has passed the mass insensitive region around the node of vibration (2nd mode), but is yet to reach the mass insensitive region closer to the mid-point of the cantilever (1st mode). As growth occurs in multiple directions it is not possible to accurately determine the exact position of all hyphal filaments at this time without the aid of optical microscopy.

Fungal growth on a 2 μm thick cantilever

A single *A. niger* spore was placed onto a cantilever sensor. Fig. 3(a) shows the resonance frequency shift for the first four flexural resonance modes once germination has occurred. Fig. 3(b) shows images taken at the start and end of the experiment. Hyphal growth has occurred in a straight line along the left side of the cantilever. For the fundamental resonance mode there is an initial negative frequency shift as growth occurs in the mass sensitive region. As the hyphal tip propagates towards the clamped end of the cantilever we see a plateau in resonance frequency, followed by a positive resonance frequency shift. A positive shift in resonance frequency indicates that the Young's modulus of the hypha in question (with a thickness that is more than double that of the cantilever) is sufficient to have a measureable effect. The higher modes of vibration also show negative and positive shifts in resonance frequency. A time lapse video of the evolution of hyphal growth on the cantilever in question can be found in the ESI (see Movie S2†).

For modes 2–4 the mass and stiffness responsivities go through maxima and minima along the cantilever length. The positions at which these occur depend on the positions of the nodes and antinodes of the vibrational mode shape (Fig. 1). The use of four modes of vibration has allowed for the propagation of the hyphal tip to be investigated in more detail than when two modes are used (7 μm thick cantilever experiment). Table 1 contains the time points where negative frequency shifts occur following a positive frequency shift. These times correspond to points (Fig. 3(a)) where the rate of frequency decrease is the greatest, and constant following a positive shift. The modes (n) from which these time points are determined are also shown. The position of the hyphal tip was determined from the images recorded during the growth measurement. The column

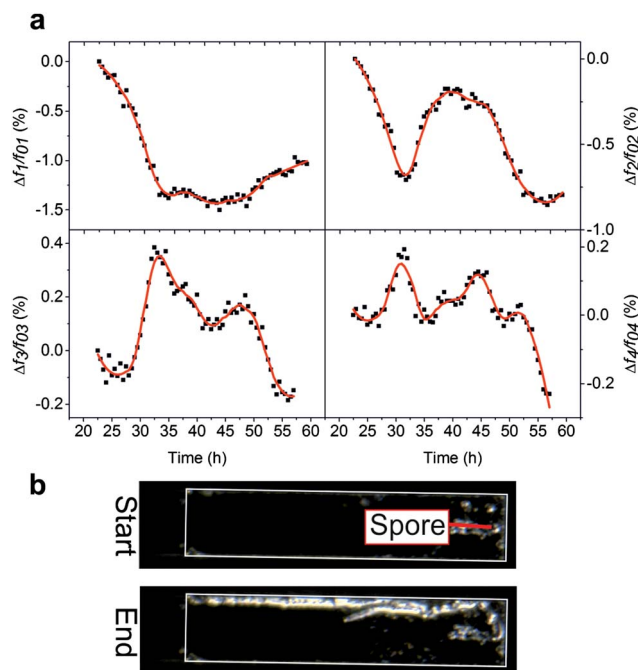


Fig. 3 Data concerning growth measurement performed using a 2 μm thick cantilever. (a) Relative resonance frequency shifts due to *A. niger* growth for the first four resonance modes. (b) Images recorded at the start and end of the growth measurement. Hyphal growth has occurred along the left side of the cantilever. The cantilever outline is shown in white. Initial spore position is also indicated.

Table 1 Table of the hypha tip position in relation to the cantilevers' free end at selected time points^a

Time (h)	n	x image (μm)	Predicted x (μm)
31.5	4	92 (± 2)–108 (± 2)	105
34	3	144 (± 2)–155 (± 2)	147
45	2	229 (± 3)–239 (± 3)	236
45.5	4	239 (± 3)–250 (± 3)	251
50	3	337 (± 4)–348 (± 4)	347
52.5	4	389 (± 4)–400 (± 5)	391

^a The time points correspond to points on plots in Fig. 3(a) where the rate of frequency decrease is the greatest and constant following a positive shift. The column ' x image' corresponds to the position of the hyphal tip before and after resonance frequency measurement at the indicated time point. The column ' x predicted' shows the positions of the maxima of the stiffness responsivity for the corresponding resonance modes.

' x image' shows the distance of the hypha tip from the cantilevers' free end. The column ' x predicted' shows the positions, from the cantilevers' free end, of the maxima of $d^2\psi_n(\delta)^2/d\delta^2$ which is proportional to the stiffness responsivity. Hence, the time points where the rate of negative frequency shift is the greatest and constant following a positive frequency shift indicates that the hyphal tip is at a position of the maximum curvature along the cantilevers' longitudinal axis. From this table it can be observed that the position of the hyphal tip can be obtained by tracking multiple higher order resonance modes

without the need for imaging. Two dimensional positioning of a growing spore tip could be envisioned on square shaped resonators. The torsional spring constant which results from using one dimensional geometry is up to 30 times higher than the deflection spring constant⁴⁰ and therefore not sensitive to the features measured here.

Simulation of hyphal growth along a 7 μm thick cantilever

We calculate the resonance frequency shift, due to hyphal growth along a cantilever's longitudinal axis, using eqn (2) and finite element modelling (FEM) to substantiate the experimental observations made. Calculations using eqn (2) were performed using Mathematica while COMSOL was used for FEM. A schematic of the modelled cantilever and hypha is shown in Fig. 4. The hypha was modelled as growing along the middle of the cantilever. The cantilever was given a length (L), width (w), and thickness (t_b) of 500, 100, and 7 μm respectively. The cantilever was assumed to have a density (ρ_b) of 2330 kg m^{-3} and a Young's modulus (E_b) of 131 GPa. The hypha was initially modelled as a rectangular block with a width, thickness (t_a), and length of 5, 5, and 10 μm respectively. Due to its high water content (>90%) the hypha was assumed to have a density (ρ_a) of 1000 kg m^{-3} and a Young's modulus (E_a) of 0.2 GPa. Resonance frequencies were calculated at a hyphal length interval (x) of 10 μm . For calculations performed using eqn (2) the hypha was modelled as consecutive rectangular blocks, where the mass of the hypha was added to that of the cantilevers to ensure that the entire mass of the biomaterial is considered as its length increases. The same was not applied to the Young's modulus of the hypha as the effect that the stiffness of an elongated mass has on cantilever's resonance frequency is not easily determined or accounted for in eqn (2). For FEM, the length of the block representing the hypha was increased in 10 μm intervals. A Poisson ratio (ν) of 0.5 was applied to the hypha and an extremely fine free tetrahedral mesh was used. Calculated relative resonance frequency shifts for the fundamental and second resonance modes are shown in Fig. 5. The shifts calculated by FEM and eqn (2) agree closely. Increasing the Young's modulus of the biomaterial in the simulation to 1 GPa results in a slight difference in the two curves towards the clamped region of the sensor (see ESI Fig. S1†). As expected, a reduction in negative frequency shifts is observed in regions where $\psi_n(x)$ is small. No positive frequency shifts are observed due to the relatively low stiffness of the hypha. When compared

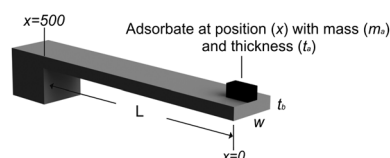


Fig. 4 Schematic of the cantilever with a hypha at position x along the cantilever's longitudinal axis. $x = 0$ corresponds to the cantilever's free end while $x = 500$ corresponds to the clamped end. L , w , and t_b correspond to the length, width, and thickness of the cantilever respectively. m_a and t_a correspond to the mass and thickness of the hypha respectively.

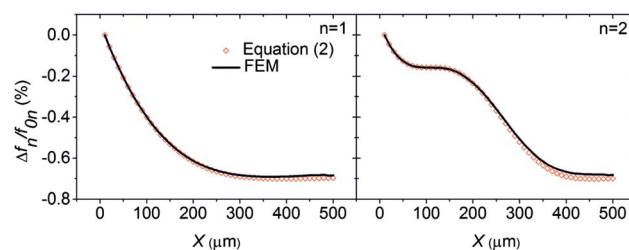


Fig. 5 Modelling of hyphal growth along the length of a 7 μm thick cantilever. Plots are shown for the fundamental and second resonance modes. Calculated frequency shifts using both methods agree. As is observed experimentally there are no negative frequency shifts observed in regions of the cantilever where vibrational amplitude is small.

to plots shown in Fig. 2, it can be seen that there is a qualitative agreement between what is observed experimentally once events such as hydrophobin production are ignored. It was not possible to obtain quantitative agreement between theory and experimental data as hyphal growth occurs in multiple directions at different rates. Videos of the evolution of the FEM simulation can be found in the ESI (see Movies S3 and S4†).

Simulation of hyphal growth along a 2 μm thick cantilever

For FEM the same material properties outlined in the previous section were applied to the cantilever beam. In order to simulate the experiment accurately the start of the block that represents the hypha was positioned on the left and 15 μm from the cantilever's free end. Initially the block representing the hypha was given the dimensions outlined previously. Through examination of recorded images it was found that approximately 145 μm from the cantilever's free end the hypha splits into two, with the resulting hyphae having a thickness that is half that of the original. Hence, for simulation the width and thickness of the hypha are changed to 2.5 μm at this position. The shorter hypha, which grows at a slower rate, is not accounted for in simulation. Applying a Young's modulus of 0.2 GPa produces trends similar to those shown in Fig. 5 with no positive frequency shifts being observed. Hence, this value was deemed to be too low as positive frequency shifts were observed experimentally (Fig. 3). Fig. 6 shows the relative frequency shifts obtained when a Young's modulus of 1 GPa was applied. This value is a factor five larger than values found in the literature, where measurements are typically performed using AFM on hyphal cell walls in a transversal direction. Anisotropic Young's modulus has been reported in plant cell walls (comparable to hyphal cell walls), where values for Young's modulus are seen to increase by a factor of four in some directions.⁴¹ The Young's modulus of DNA-protein filaments or protein filaments such as microtubuli, which were stretched along their longitudinal axis, has also been found to be in the order of 1–10 GPa.⁴² As structures similar to these are present in hyphal walls this assumed value is reasonable.

The plots shown in Fig. 6 reveal similar trends to those measured experimentally, however positive and negative frequency shifts occur at slightly different positions along the cantilever length. These discrepancies can be attributed to the use of an oversimplified model as growth does not occur in a

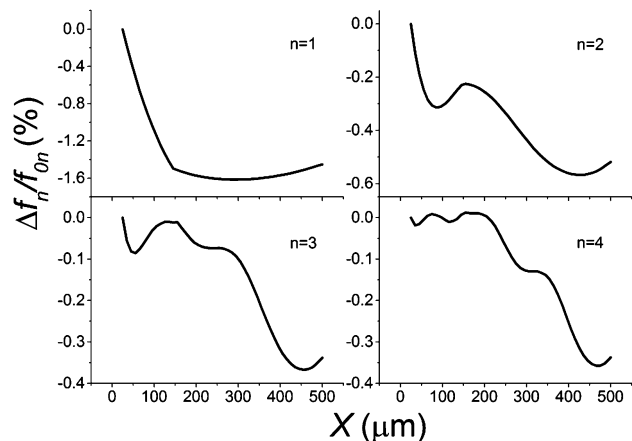


Fig. 6 FEM of hypha growth along the longitudinal axis of a 2 μm thick cantilever. Similar trends to those measured experimentally are observed, however not at the same positions.

straight line and hyphal splitting is also not accounted for. Mode shape changes were also observed during simulation, which would also contribute to discrepancies between experimental data. Videos highlighting the simulated evolution of the vibrational mode shape due to hyphal growth can be found in the ESI (see Movies S5–S8†).

Conclusion

Monitoring of the growth of single *A. niger* spores has been shown using multiple resonance modes. Growth detection times as low as 7–10 hours have been achieved. This is an order of magnitude faster than conventional growth detection techniques. These growth detection times are also in agreement with the work previously published, where single mode detection was performed.²⁹ The detection of this minimal amount of the fungal material indicates the suitability of this method for growth monitoring in any setting. The ability to detect the viability of single spores within a short time is advantageous in a clinical setting as it allows for a reduction in the number of isolates required.

The use of several higher modes allows for real time monitoring of fungal growth. It has been demonstrated that it is possible to determine the extent to which growth has proceeded along the cantilever length. In the case where growth is proceeding in a linear fashion towards the cantilevers' clamped end we show that a more accurate determination of the hyphal tip position can be performed. Events occurring on a cellular level, such as the secretion of hydrophobins, can also be detected. The measurement of such biological processes highlights the advantages that are gained through the use of cantilevers for the monitoring of microbial growth, as opposed to the use of optics based methods. While optical inspection allows for viable spore growth to be detected, it provides no information on the mechanical properties of newly grown hyphae. It is believed that the use of cantilevers will provide information on the effects that antibiotic drugs have on the mechanical

properties of complex microorganisms and microbe populations. Measurement of multiple modes also allows for the positions at which these processes occur to be determined.

We demonstrate here that cantilever arrays can be used to monitor the development of complex biological structures such as fungal hyphae. As such this method has the potential to be utilised for the assessment of other complex elongated structures (e.g. nerve cell axons) or organisms such as *Caenorhabditis elegans* (*C. elegans*). Employing higher order resonance modes or resonators with different geometries (e.g. 2D membranes) will allow for complex microbiological growth phenomena to be studied mechanically in great detail.

Materials and methods

Cantilever sensor preparation

Cantilever arrays were obtained from the IBM Research Laboratory, Rüschlikon, Switzerland. Each array consists of 8 cantilevers with a pitch of 250 μm between sensors. The cantilevers on the arrays used had a length, width, and thickness of 500 μm , 100 μm , and 2 or 7 μm respectively. Arrays were cleaned by exposure to oxygen plasma for 3 minutes using the following settings: 0.3 mbar O_2 , 160 W, and 40 kHz (PICO Barrel Asher; Diener electronic GmbH + Co. KG, Ebhausen, Germany). The arrays were immediately immersed in a silane solution (3-glycidyloxypropyltrimethoxysilane–*N* ethyldiisopropylamine–water free toluene; 1 : 1 : 100) for 45 minutes and then washed twice with water free toluene for 15 minutes. Arrays were dried under nitrogen. This step provides an epoxy activated surface which is reactive under alkali conditions towards primary hydroxyl groups found in agarose. Immediately prior to functionalisation the pH of an agarose (SeaKem Gold Agarose, Bioconcept; New Hampshire, USA) solution (1% wt/vol) was adjusted to approximately 11.9 by addition of 2 M NaOH. This facilitates epoxy coupling to agarose. The cantilevers were functionalised with the agarose biopolymer *via* a 3 second immersion in heated capillary tubes ($\sim 100^\circ\text{C}$). Arrays were subsequently immersed in the Roswell Park Memorial Institute medium broth (RPMI – 1640) which was supplemented with 0.165 M MOPS (pH = 7) and 0.2% glucose for 10 minutes in order to load the agarose layer with nutrition.

A. niger preparation

A. niger spores (CIP 1431.83; Pasteur Institute, Paris, France) were cultured on potato dextrose agar (PDA) slants at 35 $^\circ\text{C}$ for five days and then stored at 4 $^\circ\text{C}$ until required. Spores were harvested and washed with tween solution (0.01%). Spores were left to dry on a sterile glass cover slip and individual spores were subsequently transferred onto the front end of cantilevers using a glass micro-needle.

Growth measurements

Measurements are performed using a previously described device.³⁵ A USB digital camera (AM7013MZT4; Dino-Lite Europe, Netherlands) with high magnification ($\times 460$), long working distance (7.9 mm), and sufficient field of view (0.86×0.85 mm) is employed to image growth on sensors during measurements.

Environmental conditions for measurements were: 94% relative humidity and 30 °C. Resonance frequency spectra were recorded at 30 minute intervals. Images of cantilevers were captured every 30 minutes in between resonance frequency measurements.

7 μm thick sensor experiment

Frequency spectra were recorded for the first two resonance modes ($f_{01} \sim 37$ kHz and $f_{02} \sim 216$ kHz). In the case of the fundamental mode 400 data points were recorded in each spectrum at a sampling time of 8 ms per data point. For the second resonance mode 800 data points were recorded in each spectrum at 4 ms per data point. Spectra were recorded for 3 cantilevers carrying single live spores and 2 reference sensors within the array.

2 μm thick sensor experiment

Spectra were recorded for the first four resonance modes ($f_{01} \sim 9$ kHz, $f_{02} \sim 59$ kHz, $f_{03} \sim 160$ kHz, and $f_{04} \sim 295$ kHz). For the fundamental resonance mode the same spectral parameters were used as in the 7 μm thick sensor experiment. For the second resonance mode 1000 data points were recorded per spectrum with a duration of 4 ms per data point. For the third and fourth resonance modes 2000 data points were recorded in each spectrum with a duration of 2 ms per data point. Spectra were recorded for 1 cantilever carrying a single spore and 3 reference sensors within the array.

Acknowledgements

This work was supported by Science Foundation Ireland under the CSET scheme (SFI08/CE/I1432) and PI scheme (09/IN.1/B2623).

References

- 1 C. L. Moser and B. K. Meyer, *AAPS PharmSciTech*, 2011, **12**, 222–226.
- 2 L. De Vuyst, G. Vrancken, F. Ravyts, T. Rimaux and S. Weckx, *Food Microbiol.*, 2009, **26**, 666–675.
- 3 T. Sue, V. Obolonkin, H. Griffiths and S. G. Villas-Bôas, *Appl. Environ. Microbiol.*, 2011, **77**, 7605–7610.
- 4 A. D. Taylor, J. Ladd, Q. Yu, S. Chen, J. Homola and S. Jiang, *Biosens. Bioelectron.*, 2006, **22**, 752–758.
- 5 R. Daly, S. Kumar, G. Lukacs, K. Lee, A. Weidlich, M. Hegner and G. S. Duesberg, *J. Sens.*, 2012, 219485.
- 6 M. A. Cooper and V. T. Singleton, *J. Mol. Recognit.*, 2007, **20**, 154–184.
- 7 G. Binnig, C. F. Quate and C. Gerber, *Phys. Rev. Lett.*, 1986, **56**, 930.
- 8 J. Barnes, R. Stephenson, M. Welland, C. Gerber and J. Gimzewski, *Nature*, 1994, **372**, 79–81.
- 9 T. Thundat, R. Warmack, G. Chen and D. Allison, *Appl. Phys. Lett.*, 1994, **64**, 2894–2896.
- 10 M. K. Ghatkesar, T. Braun, V. Barwich, J. P. Ramseyer, C. Gerber, M. Hegner and H. P. Lang, *Appl. Phys. Lett.*, 2008, **92**, 043106.
- 11 J. Jensen, N. Maloney and M. Hegner, *Sens. Actuators, B*, 2013, **183**, 388–394.
- 12 M. K. Ghatkesar, V. Barwich, T. Braun, J.-P. Ramseyer, C. Gerber, M. Hegner, H. P. Lang, U. Drechsler and M. Despont, *Nanotechnology*, 2007, **18**, 445502.
- 13 M. Li, H. X. Tang and M. L. Roukes, *Nat. Nanotechnol.*, 2007, **2**, 114–120.
- 14 Y. Arntz, J. Seelig, H. Lang, J. Zhang, P. Hunziker, J. Ramseyer, E. Meyer, M. Hegner and C. Gerber, *Nanotechnology*, 2003, **14**, 86.
- 15 N. Backmann, C. Zahnd, F. Huber, A. Bietsch, A. Plückthun, H.-P. Lang, H.-J. Güntherodt, M. Hegner and C. Gerber, *Proc. Natl. Acad. Sci. U. S. A.*, 2005, **102**, 14587–14592.
- 16 J. Fritz, M. Baller, H. Lang, H. Rothuizen, P. Vettiger, E. Meyer, H.-J. Güntherodt, C. Gerber and J. Gimzewski, *Science*, 2000, **288**, 316–318.
- 17 F. Huber, H. Lang, N. Backmann, D. Rimoldi and C. Gerber, *Nat. Nanotechnol.*, 2013, **8**, 125–129.
- 18 B. Ilic, Y. Yang and H. Craighead, *Appl. Phys. Lett.*, 2004, **85**, 2604–2606.
- 19 T. Braun, M. K. Ghatkesar, N. Backmann, W. Grange, P. Boulanger, L. Letellier, H.-P. Lang, A. Bietsch, C. Gerber and M. Hegner, *Nat. Nanotechnol.*, 2009, **4**, 179–185.
- 20 A. Gupta, D. Akin and R. Bashir, *J. Vac. Sci. Technol., B: Microelectron. Nanometer Struct.–Process., Meas., Phenom.*, 2004, **22**, 2785–2791.
- 21 H. Sharma and R. Mutharasan, *Biosens. Bioelectron.*, 2013, **45**, 158–162.
- 22 J. W. Yi, W. Y. Shih, R. Mutharasan and W.-H. Shih, *J. Appl. Phys.*, 2003, **93**, 619–625.
- 23 T.-R. J. Tzeng, Y. R. Cheng, R. Saeidpourazar, S. S. Aphale and N. Jalili, *J. Heat Transfer*, 2011, **133**, 011012.
- 24 G. Longo, L. Alonso-Sarduy, L. M. Rio, A. Bizzini, A. Trampuz, J. Notz, G. Dietler and S. Kasas, *Nat. Nanotechnol.*, 2013, **8**, 522–526.
- 25 Y. Liu, L. M. Schweizer, W. Wang, R. L. Reuben, M. Schweizer and W. Shu, *Sens. Actuators, B*, 2013, **178**, 621–626.
- 26 A. J. Detzel, G. A. Campbell and R. Mutharasan, *Sens. Actuators, B*, 2006, **117**, 58–64.
- 27 S. Xu and R. Mutharasan, *Anal. Chem.*, 2011, **83**, 1480–1483.
- 28 K. Y. Gfeller, N. Nugaeva and M. Hegner, *Appl. Environ. Microbiol.*, 2005, **71**, 2626–2631.
- 29 N. Maloney, G. Lukacs, N. Nugaeva, W. Grange, J. Ramseyer, J. Jensen and M. Hegner, *J. Sens.*, 2012, 405281.
- 30 N. Nugaeva, K. Gfeller, N. Backmann, H. P. Lang, H. J. Guntherodt and M. Hegner, *Microsc. Microanal.*, 2007, **13**, 13–17.
- 31 G. Lukacs, N. Maloney and M. Hegner, *J. Sens.*, 2012, 561256.
- 32 J. Tamayo, P. M. Kosaka, J. J. Ruz, A. San Paulo and M. Calleja, *Chem. Soc. Rev.*, 2013, **42**, 1287–1311.
- 33 D. Ramos, J. Tamayo, J. Mertens, M. Calleja and A. Zaballos, *J. Appl. Phys.*, 2006, **100**, 106105.
- 34 D. Ramos, J. Tamayo, J. Mertens, M. Calleja, L. Villanueva and A. Zaballos, *Nanotechnology*, 2008, **19**, 035503.
- 35 N. Maloney, G. Lukacs, S. Ball and M. Hegner, *Rev. Sci. Instrum.*, 2014, **85**, 015003.
- 36 T. Tsukahara, *Med. Mycol.*, 1968, **6**, 185–191.

- 37 D. Gottlieb and R. Tripathi, *Mycologia*, 1968, 571–590.
- 38 J. Bayry, V. Aimanianda, J. I. Guijarro, M. Sunde and J.-P. Latge, *PLoS Pathogens*, 2012, **8**, e1002700.
- 39 H. A. Wösten, M.-A. van Wetter, L. G. Lugones, H. C. van der Mei, H. J. Busscher and J. G. Wessels, *Curr. Biol.*, 1999, **9**, 85–88.
- 40 S. Jeon, Y. Braiman and T. Thundat, *Appl. Phys. Lett.*, 2004, **84**, 1795–1797.
- 41 C. Wei, L. S. Lintilhac and P. M. Lintilhac, *Planta*, 2006, **223**, 1058–1067.
- 42 M. Hegner, S. B. Smith and C. Bustamante, *Proc. Natl. Acad. Sci. U. S. A.*, 1999, **96**, 10109–10114.